Advanced Robotics
Publication details, including instructions for authors and subscription information:
http://www.tandfonline.com/loi/tadr20

Position and stiffness analysis of a new asymmetric 2PRR-PPR parallel CNC machine

Amir Rezaei [a] & Alireza Akbarzadeh [a]
[a] Center of Excellence on Soft Computing and Intelligent Information Processing, SCIIP, Mechanical Engineering Department, Ferdowsi University of Mashhad, Mashhad, Iran
Version of record first published: 03 Jan 2013.

To cite this article: Amir Rezaei & Alireza Akbarzadeh (2013): Position and stiffness analysis of a new asymmetric 2PRR-PPR parallel CNC machine, Advanced Robotics, 27:2, 133-145

To link to this article: http://dx.doi.org/10.1080/01691864.2013.751154

Advanced Robotics, 2013
Vol. 27, No. 2, 133–145, http://dx.doi.org/10.1080/01691864.2013.751154

Taylor & Francis
Taylor & Francis Group

FULL PAPER

Position and stiffness analysis of a new asymmetric 2PRR–PPR parallel CNC machine

Amir Rezaei and Alireza Akbarzadeh*

Center of Excellence on Soft Computing and Intelligent Information Processing, SCIIP, Mechanical Engineering Department, Ferdowsi University of Mashhad, Mashhad, Iran

(*Received 13 December 2011; accepted 9 February 2012*)

In this paper, structural stiffness analysis of a new 3-axis asymmetric planar parallel manipulator, a 2PRR–PPR structural kinematic chain, is investigated. The manipulator is proposed as a tool holder for a 5-axis hybrid computer numerical control (CNC) machine. First, the structure of the robot is introduced and inverse kinematics solution is presented. Secondly, stiffness matrix of the robot is determined using a continuous method based on Castigliano's theorem and calculation of strain energy of the robot components. This method removes the need for commonly used simplifying assumptions and, therefore, results in good accuracy. For this purpose, force and strain energy for each segment of the robot are analyzed. Finally, to verify the analytical results, commercial FEM software is used to simulate the physical structure of the manipulator. A numerical example is presented which confirms the correctness of the analytical formulations.

Keywords: asymmetric parallel robot; inverse kinematic; stiffness matrix; distributed model; FEA

1. Introduction

Nowadays, the application of parallel robots is developing. Examples include implementation in many engineering fields such as simulations, aerospace, cutting, welding, surgical, and computer numerical control (CNC) machines [1,2]. Most machine tools use serial kinematic chains as their spindle [1,3,4]. The serial structures of these mechanisms usually have low payloads and are sensitive to vibrations [5,6]. On the other hand, parallel robots usually offer high precision, high stiffness, and high load carrying capacity as well as good dynamic efficiency over their serial counterparts [7,8,9]. These advantages are the reasons why parallel robots are being considered for CNC machine tools [6,9,10]. The principal disadvantage of parallel robots is that they have smaller workspace than serial counterparts [11,9]. Generally, a parallel manipulator is composed of a moving platform which is connected to a fixed base by several parallel legs. The heavy actuators are commonly placed at the fixed base. Therefore, these manipulators are inherently stiffer and more accurate and can offer higher speed than their serial counterparts [10,12,13]. Robot accuracy, in general, has a direct relationship with its structural stiffness. When parallel robots are used as a CNC machine tool, structural stiffness is considered one of the most important and fundamental design parameters [3,14–16]. High structural stiffness can increase precision of the machining process [17]. To study robot stiffness, its related stiffness matrix must be determined [5,18]. Stiffness matrix indicates a relationship between vector of a small displacement of the end-effector and vector of static force/moment (wrench) applied at that point [18–20].

In recent years, many studies have been presented on structural stiffness of parallel manipulators. Rezaei and Akbarzadeh [1,18] presented stiffness analysis of a spatial 3-PSP parallel robot with flexible moving platform using a continuous method based on Castigliano's theorem. Also, Enferadi and Akbarzadeh [5] investigated the stiffness of a spherical parallel robot using calculation of strain energy of each component of the robot. Li and Xu derived instinctively the stiffness matrix of a 3-PUU parallel kinematic machine based on an alternative approach considering actuations and constraints [11]. Kim investigated the stiffness analysis of a 3-DOF parallel robot with one constraining leg while considering elastic deformations of joints and links. They obtained the overall stiffness matrix using Jacobian matrix and principle of virtual work [6].

In the present investigation, a new 3-axis asymmetric planar parallel robot with a 2PRR–PPR structural kinematic chain as a tool holder in a CNC machine tool is presented. To obtain stiffness, a method based on Castigliano's theorem and calculation of strain energy for the robot components is presented. Using this method, robot components are modeled as distributed. Traditional methods for obtaining stiffness use many assumptions

*Corresponding author. Email: ali_akbarzadeh@um.ac.ir

for simplification of the model, such as assuming lumped models for the robot components. On the other hand, when a robot is modeled as distributed, there is no need for many of the simplifying assumptions. Furthermore, the proposed method allows considering bending in all robot components. This approach increases model accuracy. In the present investigation, a FEM model is also generated to verify the derived theoretical model and demonstrate its accuracy.

2. Structure of a new asymmetric planar parallel robot

In this paper, a new asymmetric planar parallel manipulator with a 2PRR–PPR structural kinematic chain is introduced. This manipulator is suggested as a 3-DOFs planar spindle holder for a 5-axis hybrid CNC milling machine. The asymmetric manipulator plus an additional two axis work table construct the hybrid CNC machine. The solid model of this robot is illustrated in Figures 1 and 2. The three DOFs of the robot consist of two translational along y and z-axes and one rotational DOF about x-axis. This robot is composed of a moving platform which is shaped like a symmetrical triangle. The moving platform is connected to a fixed base with two double parallel bars, AR_1 and BR_2, and one horizontal double guide rods, $N_{31}N_{32}$ (see Figure 3). These components are connected to the fixed base by four moving blocks, N_i. Thus, this robot consists of two PRR and one PPR serial kinematic chains. The first prismatic joint in PRR and the second prismatic joint in PPR are the actuated joints. Therefore, the structural kinematic chain of this robot may be expressed by 2PRR−PPR.

3. Inverse kinematic solution

For a given manipulator, stiffness changes with the variation of the manipulator configurations within its workspace [1,18]. Therefore, it is necessary to investigate the kinematic behavior of a manipulator in its different configurations. For this purpose, we will obtain the inverse kinematics solution of the presented parallel manipulator. Figure 3 shows geometry for a typical kinematic chain of the robot. Vectors and reference frames used are

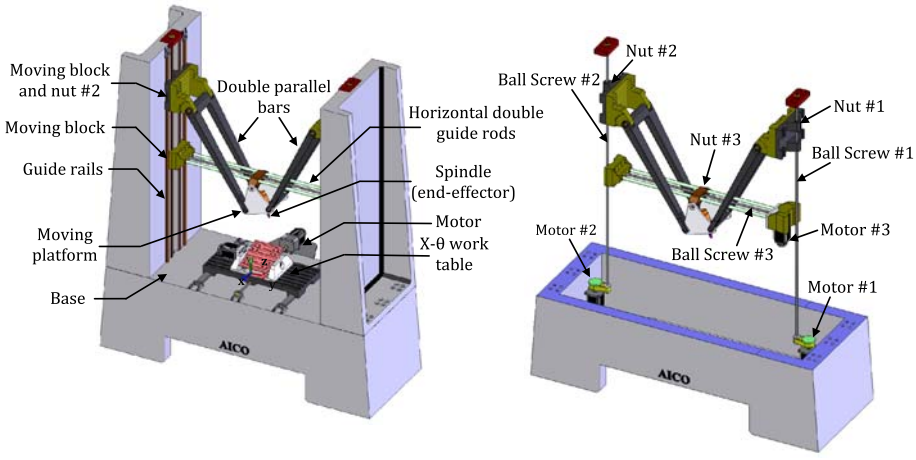

Figure 1. The solid model of the asymmetric parallel CNC machine.

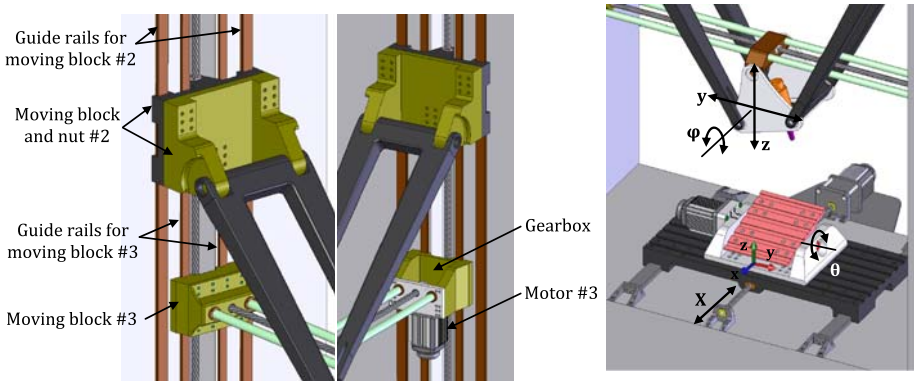

Figure 2. Details of ball screw-nut assembly and DOFs.

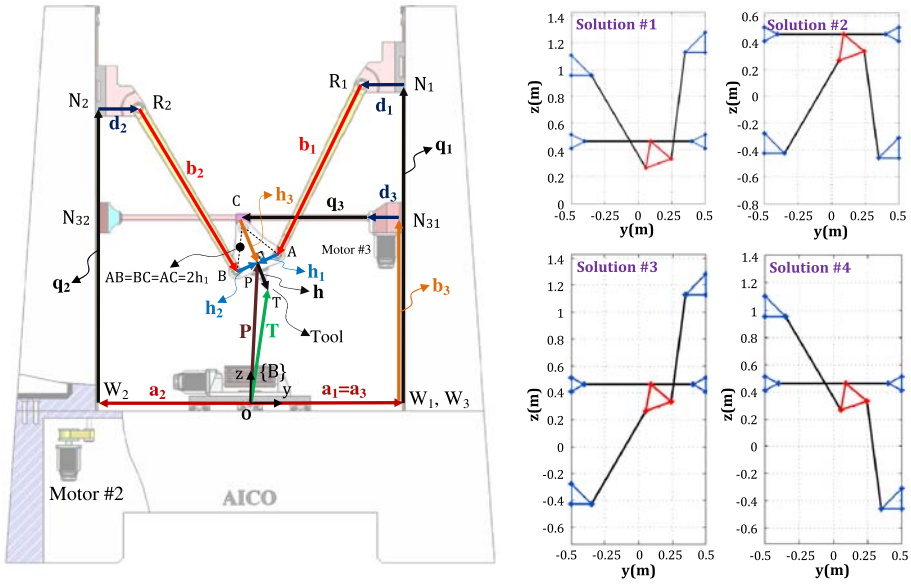

Figure 3. Close vector loops for the PPR and the PRR kinematic chains and the four inverse kinematics solutions.

described in this figure. A nonmoving base coordinate frame {B} is attached at point O. As shown in Figure 3, positions of nuts are denoted by three position vectors $\mathbf{q}_i$. Position of the end-effector, point P, is given by vector $P = [y_P \; z_P]^T$. Also, the angle φ represents the orientation angle of the moving platform about the x-axis.

The inverse kinematics obtains the actuated variables, q_i, from a given position, point P, and orientation, φ, of the moving platform. To solve the inverse kinematic problem, a close vector-loop is written for each kinematic chain as

$$\mathbf{T} = \mathbf{a}_i + \mathbf{q}_i + \mathbf{d}_i + \mathbf{b}_i + \mathbf{h}_i + \mathbf{h} \quad i = 1, 2, 3 \tag{1}$$

$$\mathbf{T} = \mathbf{P} + \mathbf{h} \tag{2}$$

Therefore, the three kinematics closed loops are:

$$i = 1 \quad \text{loop}\#1\text{:}\,\text{OW}_1\text{N}_1\text{R}_1\text{APT} \tag{2a}$$

$$i = 2 \quad \text{loop}\#3\text{:}\,\text{OW}_2\text{N}_2\text{R}_2\text{BPT} \tag{2b}$$

$$i = 3 \quad \text{loop}\#2\text{:}\,\text{OW}_1\text{N}_{31}\text{CPT} \tag{2c}$$

As shown in Figure 3, we can write, $a_1 = a_2 = a_3 = a$. For the inverse kinematic solution, position of the end-effector and orientation of the moving platform are specified. In other words, the vector $\mathbf{P}$ and value of φ are defined. Subsequently, the values of y_p and z_p are known. Thus, the position values of points A, B, and C (corner position of the moving platform) can be written as

$$z_A = z_P + h_1 \sin\varphi, \quad y_A = y_P + h_1 \cos\varphi \tag{3a}$$

$$z_B = z_P - h_2 \sin\varphi, \quad y_B = y_P - h_1 \cos\varphi \tag{3b}$$

$$z_C = z_P + h_3 \cos\varphi, \quad y_C = y_P - h_3 \sin\varphi \tag{3c}$$

By substituting Equations (3) and values for the kinematics constants a, b_1, and d_1, d_2 and d_3 into Equations (1) and (2), the position of each nut is obtained as follows

$$q_1 = z_A \pm \sqrt{b_1^2 - (a_1 - d_1 - y_A)^2} \tag{4a}$$

$$q_2 = z_B \pm \sqrt{b_2^2 - (a_2 - d_2 - y_B)^2} \tag{4b}$$

$$q_3 = a_3 - d_3 - y_C \tag{4c}$$

Upon solving these equations, Equations (4), four solutions for a given position and orientation of the robot are obtained. These four solutions correspond to four configurations of the robot. However, considering Figure 3, only one of these answers is correct and can be used in the machining process.

4. Stiffness analysis

In this section, the development of the robot stiffness matrix is presented. Stiffness analysis measures small deflection of robot's end-effector when external wrench is applied to this point [1,5]. This relationship is expressed by stiffness matrix which requires finding the

relationship between the applied external wrench on the end-effector and the resultant forces in each component of the robot. Various methods are suggested for obtaining the stiffness matrix [6,10–15]. These methods are mostly based on modeling the robot components as lumped and use the principle of virtual work to obtain the stiffness matrix. The simplifying assumptions used in the process of modeling the robot stiffness, such as lumped model, results in loss of accuracy in stiffness calculation [18]. In this paper, a continuous method is used for obtaining the manipulator stiffness matrix which is based on Castigliano's theorem and calculation of strain energy due to flexibility of the robot components. To do this first, inverse kinematic and force analysis are performed. Next, using Castigliano's theorem, stiffness matrix is obtained. The following assumptions are used:

- The moving platform is assumed to be rigid.
- Weights and friction of joints are negligible.
- Weights of all robot components are assumed negligible.

4.1. Force analysis

In this subsection, the relationship between the applied external wrench on the end-effector, point *P*, as well as the resultant joints forces are developed. From force analysis, several analytical expressions will be obtained that will allow calculation of reaction forces. Consider Figure 4. The external wrench $\mathbf{W}$ can be defined in the fixed base {B} as follow

$$\mathbf{W} = [\mathbf{f}_{\text{ext}}\ \mathbf{M}_{\text{ext}}]^{\text{T}}, \quad \mathbf{f}_{\text{ext}} = [f_y\ f_z]^{\text{T}}, \quad \mathbf{M}_{\text{ext}} = M_{\text{X}} \tag{5}$$

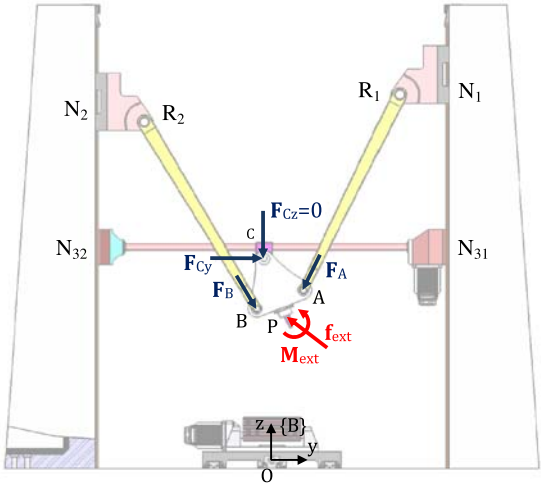

Figure 4. Free body diagram (FBD) of the moving platform.

Where, $\mathbf{f}_{\text{ext}}$ denotes a force vector and $\mathbf{M}_{\text{ext}}$ denotes a moment about *x*-axis.

As shown in Figure 4, the reaction forces are obtained as

$$\sum \mathbf{F} = F_{\text{A}}\hat{\mathbf{e}}_{b1} + F_{\text{B}}\hat{\mathbf{e}}_{b2} + F_{\text{C}y}\hat{\mathbf{e}}_y + \mathbf{f}_{\text{ext}} = \mathbf{0} \tag{6a}$$

$$\begin{aligned}\sum \mathbf{M}_P = {} & F_{\text{A}}h_1(\hat{\mathbf{e}}_{h1} \times \hat{\mathbf{e}}_{b1}) + F_{\text{B}}h_2(\hat{\mathbf{e}}_{h2} \times \hat{\mathbf{e}}_{b2}) \\ & + F_{\text{C}}h_3(\hat{\mathbf{e}}_{h3} \times \hat{\mathbf{e}}_y) + M_{\text{ext}} \\ = {} & 0\end{aligned} \tag{6b}$$

In Equations 6(a) and (b), the unit vectors along the reaction forces may be represented as follows

$$\hat{\mathbf{e}}_{b1} = \frac{b_1}{|b_1|}, \mathbf{b}_1 = [(y_{\text{A}} - a_1 + d_1)\ \ (z_{\text{A}} - q_1)]^T \tag{7a}$$

$$\hat{\mathbf{e}}_{b2} = \frac{b_2}{|b_2|}, \mathbf{b}_2 = [(y_{\text{B}} - a_2 - d_2)\ \ (z_{\text{B}} - q_2)]^T \tag{7b}$$

$$\hat{\mathbf{e}}_{h1} = \frac{h_1}{|h_1|}, \mathbf{h}_1 = [(y_{\text{P}} - y_{\text{A}})\ \ (z_{\text{P}} - Z_{\text{A}})]^T \tag{7c}$$

$$\hat{\mathbf{e}}_{h2} = \frac{h_2}{|h_2|}, \mathbf{h}_2 = [(y_{\text{P}} - y_{\text{B}})\ \ (z_{\text{P}} - Z_{\text{B}})]^T \tag{7d}$$

$$\hat{\mathbf{e}}_{h3} = \frac{h_3}{|h_3|}, \mathbf{h}_3 = [(y_{\text{P}} - y_{\text{C}})\ \ (z_{\text{P}} - Z_{\text{C}})]^T \tag{7e}$$

$$\hat{\mathbf{e}}_y = [1\ \ 0]^T \tag{7f}$$

Directions of these unit vectors change due to configuration of the robot. Therefore, directions of the unit vectors are determined by inverse kinematics problem. By simplifying the above equations, relation between external wrench and reaction forces in matrix form are obtained as

$$\mathbf{W} = \mathbf{A}_{3\times3}\mathbf{F}_{\text{reaction}}, \mathbf{F}_{\text{reaction}} = [F_A\ F_B\ F_{Cy}]^T \tag{8}$$

where,

$$\mathbf{A}_{3\times3} = -\begin{bmatrix} l[\hat{\mathbf{e}}_{b1}\ \ \hat{\mathbf{e}}_{b2}\ \ \hat{\mathbf{e}}_y]_{2\times3} \\ h_1(\hat{\mathbf{e}}_{h1} \times \hat{\mathbf{e}}_{b1})h_2(\hat{\mathbf{e}}_{h2} \times \hat{\mathbf{e}}_{b2})h_3(\hat{\mathbf{e}}_{h3} \times \hat{\mathbf{e}}_y)] \end{bmatrix} \tag{9}$$

To obtain the reaction forces given the applied external wrench, Equation (8) can be written as follow

$$\mathbf{F}_{\text{reaction}} = \mathbf{B}_{3\times3}\mathbf{W}, \quad \mathbf{B}_{3\times3} = \mathbf{A}_{3\times3}^{-1}, \quad \mathbf{B}_{3\times3} = \text{B}_{ij} \tag{10}$$

4.2. Stiffness matrix determination

In this subsection, strain energy of each component of the robot is calculated. To do this, force analysis and inverse position analysis are used. The total strain energy of the 2PRR−PPR manipulator can be written as

$$U = U_{\text{link}(AR_1)} + U_{\text{link}(BR_2)} + U_{\text{motors}} \tag{11}$$

where, U is total strain energy of robot which is equal to sum of strain energies due to all links and the three motors. The overall stiffness matrix, $\mathbf{K}$ which is the mapping between applied external wrench and infinitesimal rotational and translational displacement of the end-effector, can be written as

$$\mathbf{W} = \mathbf{K}\delta\mathbf{S}_P \tag{12}$$

where, $\mathbf{W}$ represents overall vector of the external wrench applied to the end-effector, CNC tool. Additionally, $\delta\mathbf{S}_P$ represents overall infinitesimal twist of the tool which is made up virtual translations, δS_y, δS_z and virtual rotation δS_φ, along y, z, and about x-axis, respectively. By the Castigliano's theorem, we can write

$$\delta\mathbf{S}_P = [\delta S_y \quad \delta S_z \quad \delta S_\varphi]^T = \begin{bmatrix} \frac{\partial U}{\partial f_y} & \frac{\partial U}{\partial f_z} & \frac{\partial U}{\partial M_x} \end{bmatrix} = \mathbf{C}\mathbf{W} \tag{13}$$

where, $\mathbf{C}$ is overall compliance matrix of the asymmetric parallel manipulator. Comparing Equations (12) and (13), we can obtain

$$\mathbf{K} = \mathbf{C}^{-1} \tag{14}$$

According to Equation (14), to obtain the overall stiffness matrix, $\mathbf{K}$, the related compliance of all robot components must first be determined. Next, using Equation (13), infinitesimal twist of the tool corresponding to the applied external wrench at this point can be calculated.

4.3. Obtaining the overall compliance matrix of the manipulator

As shown in Figure 5, the two double parallel bars, AR_1 and BR_2 experience reaction forces as axial forces. Therefore, to calculate the strain energy of these components due to applied external wrench, we can write

$$U_{\text{links}(AR_1)} = \int_0^{b_1} \frac{F_A^2}{4A_1(x)E}\,dx, \qquad 0 \le x \le b_1 \tag{15a}$$

$$U_{\text{links}(BR_2)} = \int_0^{b_2} \frac{F_B^2}{4A_2(x)E}\,dx, \qquad 0 \le x \le b_2 \tag{15b}$$

Where, F_A and F_B are the axial reaction forces in joints A and B due to applied external wrench, respectively. These forces are determined from solving the force analysis and inverse kinematics problem, simultaneously. To maintain generality, the cross-section areas, $A_1(x)$ and $A_2(x)$ are defined by a function $A_1 = A_2(x) = A_2(x)$. Referring to Figure 6, the function representing the cross-sectional area for each of the double parallel bar is defined as

$$A(x) = A_{(x=0)} - \left(\frac{A_{(x=0)} - A_{(x=b)}}{b}\right)x \tag{16}$$

where, $b_1 = b_2 = b = 0.8\,\text{m}$ and $A_{(x=0)} = 0.00356\,\text{m}^2$ and $A_{(x=b)} = 0.00163\,\text{m}^2$. Therefore, the function for the cross-sectional area, $A(x)$, is calculated as

$$A(x) = 0.00356 - 0.00241x \tag{17}$$

To calculate the strain energy due to flexibility of the motors, the relationship between axial forces acting at the end of each rod and its resulting motor torque should be found. The motor and ball screw assembly of each axis are shown in Figure 7. It should be noted that the present investigation does not consider the influence of friction and body weight. Therefore, F_{Cz} and $F_{\text{friction}} = 0$.

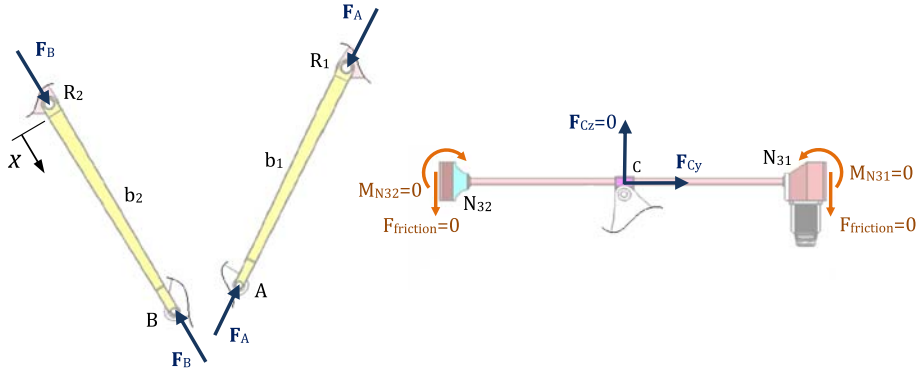

Figure 5. The FBDs for the two double parallel bars and the clamped–clamped double beam.

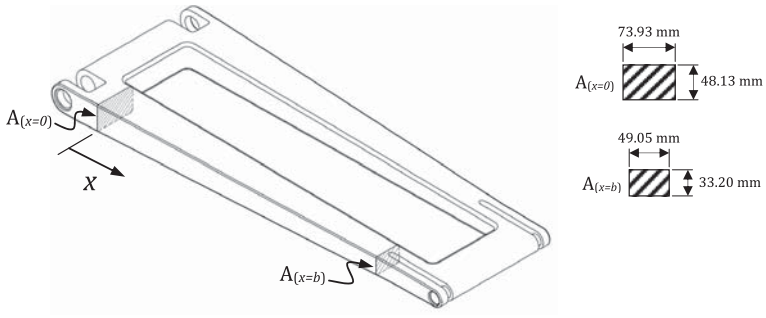

Figure 6. Isometric view of the double parallel bar-determination of the function for cross-sectional area.

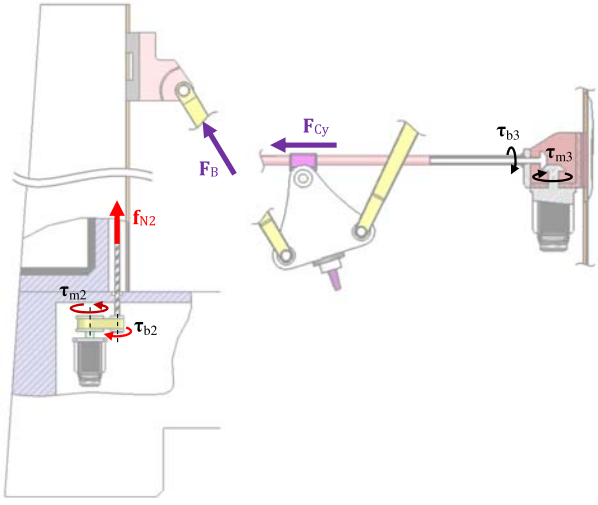

Figure 7. Free body diagrams for the motor and ball screw assembly #2 and #3.

The relationship between the resistant torque in the motor and the corresponding axial force, f_{Ni}, can be written as

$$\tau_{\mathrm{mi}} = \frac{\mathrm{N} l_b}{2\pi} f_{\mathrm{Ni}} \tag{18}$$

where, τ_{mi} is the resistant torque in the ith motor due to axial force, f_{Ni}, acting on the ith axis of the robot. The gearbox transmission ratio for the robot is selected to be $N=2$ and l_b represents the lead of the ball screw. Strain energy of the three motors can be written as

$$U_{\mathrm{motors}} = U_{\mathrm{motors}(N_1)} + U_{\mathrm{motors}(N_2)} + U_{\mathrm{motors}(N_3)} \tag{19}$$

where,

$$U_{\mathrm{motors}(N_i)} = \sum_{i=1}^{3} \left(\frac{\tau_{\mathrm{mi}^2}}{2k_{\mathrm{tor},i}} \right) = \frac{N^2 l_{b^2}}{8\pi^2} \sum_{i=1}^{3} \frac{(f_{Ni})^2}{k_{\mathrm{tor},i}} \tag{20}$$

where, $k_{\mathrm{tor},i}$ is equivalent torsional stiffness of the ith motor. The axial forces, f_{Ni} are determined as

$$f_{N1} = F_A \left(\frac{q_1 - z_{\mathrm{A}}}{b_1} \right) = \left(\frac{q_1 - z_{\mathrm{A}}}{b_1} \right) \mathbf{B}_{1j}\ \mathbf{W} \tag{21a}$$

$$f_{N2} = F_B \left(\frac{q_2 - z_{\mathrm{B}}}{b_2} \right) = \left(\frac{q_2 - z_{\mathrm{B}}}{b_2} \right) \mathbf{B}_{2j}\ \mathbf{W} \tag{21b}$$

$$f_{N3} = F_{\mathrm{Cy}} = \mathbf{B}_{3j}\ \mathbf{W} \tag{21c}$$

Therefore, the overall strain energy, U, is calculated using Equation (11). Considering Equation (13) and Castigliano's theorem, the infinitesimal displacement vector components of point P can be obtained as

$$\begin{aligned} \delta S_y &= \frac{\partial U}{\partial f_y} \\ &= \int_0^{b_1} \frac{F_{\mathrm{A}}}{2\mathrm{A}(x)E} \frac{\partial F_{\mathrm{A}}}{\partial f_y} \mathrm{d}x + \int_0^{b_2} \frac{F_{\mathrm{B}}}{2A(x)E} \frac{\partial F_{\mathrm{B}}}{\partial f_y} \mathrm{d}x \\ &\quad + \frac{N^2 l_{b^2}}{4\pi^2} \sum_{i=1}^{3} \frac{f_{Ni}}{k_{\mathrm{tor},i}} \frac{\partial f_{Ni}}{\partial f_y} \end{aligned} \tag{22a}$$

$$\begin{aligned} \delta S_z &= \frac{\partial U}{\partial f_z} \\ &= \int_0^{b_1} \frac{F_{\mathrm{A}}}{2\mathrm{A}(x)E} \frac{\partial F_{\mathrm{A}}}{\partial f_z} \mathrm{d}x + \int_0^{b_2} \frac{F_{\mathrm{B}}}{2A(x)E} \frac{\partial F_{\mathrm{B}}}{\partial f_z} \mathrm{d}x \\ &\quad + \frac{N^2 l_b^2}{4\pi^2} \sum_{i=1}^{3} \frac{f_{Ni}}{k_{\mathrm{tor},i}} \frac{\partial f_{Ni}}{\partial f_z} \end{aligned} \tag{22b}$$

$$\begin{aligned} \delta S_\varphi &= \frac{\partial U}{\partial M_x} \\ &= \int_0^{b_1} \frac{F_{\mathrm{A}}}{2\mathrm{A}(x)E} \frac{\partial F_{\mathrm{A}}}{\partial M_x} \mathrm{d}x + \int_0^{b_2} \frac{F_{\mathrm{B}}}{2A(x)E} \frac{\partial F_{\mathrm{B}}}{\partial M_x} \mathrm{d}x \\ &\quad + \frac{N^2 l_b^2}{4\pi^2} \sum_{i=1}^{3} \frac{f_{Ni}}{k_{\mathrm{tor},i}} \frac{\partial f_{Ni}}{\partial M_x} \end{aligned} \tag{22c}$$

By substituting the components of matrix **B** from Equation (10), integrating and factoring the applied

external wrench, **W**, the overall compliance matrix of the robot can be expressed as

$$\delta S_y = \left(\frac{161.816}{E}(\mathrm{B}_{11}\mathbf{B}_{1j} + \mathrm{B}_{21}\mathbf{B}_{2j}) + \frac{N^2 l_b^2}{4\pi^2 k_{\mathrm{tor}}}\left(\left(\frac{q_1 - z_{\mathrm{A}}}{b_1}\right)^2 \mathrm{B}_{11}\mathbf{B}_{1j} + \left(\frac{q_2 - z_{\mathrm{B}}}{b_2}\right)\mathrm{B}_{21}\mathbf{B}_{2j} + \mathrm{B}_{33}\mathbf{B}_{3j}\right)\right)\mathbf{W} = \mathbf{C}_{1j}\mathbf{W} \quad (23a)$$

$$\delta S_z = \left(\frac{161.816}{E}(\mathrm{B}_{12}\mathbf{B}_{1j} + \mathrm{B}_{22}\mathbf{B}_{2j}) + \frac{N^2 l_b^2}{4\pi^2 k_{\mathrm{tor}}}\left(\left(\frac{q_1 - z_{\mathrm{A}}}{b_1}\right)^2 \mathrm{B}_{12}\mathbf{B}_{1j} + \left(\frac{q_2 - z_{\mathrm{B}}}{b_2}\right)\mathrm{B}_{22}\mathbf{B}_{2j} + \mathrm{B}_{33}\mathbf{B}_{3j}\right)\right)\mathbf{W} = \mathbf{C}_{3j}\mathbf{W} \quad (23b)$$

$$\delta S_\varphi = \left(\frac{161.816}{E}(\mathrm{B}_{13}\mathbf{B}_{1j} + \mathrm{B}_{23}\mathbf{B}_{2j}) + \frac{N^2 l_b^2}{4\pi^2 k_{\mathrm{tor}}}\left(\left(\frac{q_1 - z_{\mathrm{A}}}{b_1}\right)^2 \mathrm{B}_{11}\mathbf{B}_{1j} + \left(\frac{q_2 - z_B}{b_2}\right)\mathrm{B}_{23}\mathbf{B}_{2j} + \mathrm{B}_{33}\mathbf{B}_{3j}\right)\right)\mathbf{W} = \mathbf{C}_{3j}\mathbf{W} \quad (23c)$$

Using Equation (13) and Equations (23a)–(23c), the overall compliance matrix **C** can be written as

$$\mathbf{C}_{3\times 3} = \begin{bmatrix} \mathbf{C}_{1j} \\ \mathbf{C}_{2j} \\ \mathbf{C}_{3j} \end{bmatrix} \quad (24)$$

where, $\mathbf{C}_{1j}$, $\mathbf{C}_{2j}$, and $\mathbf{C}_{3j}$ represent the first, second, and third rows of matrix **C**. The elements of the matrix **B** are also determined using inverse kinematics and force analysis. Then, the overall stiffness matrix, **K,** is obtained using Equation (14). Finally, using Equation (13) and the external wrench on point *P*, the values of infinitesimal displacement of point *P* are obtained.

5. Finite element analysis

A finite element commercial software is used to evaluate the correctness of the analytical method. In the present study, element type, BEAM3 is used to develop Finite element analysis (FEA) model for the compliant components. Furthermore, the revolute and prismatic joints are assumed rigid and are modeled using MPC184 element type. For finite element modeling of the robot, stiffness of the *i*th motor, K_{mi}, is approximated with a linear spring with deformation along their ball screw's axis (see Figure 8). Consider the reaction forces on revolute joints A, B, and C. The axial forces will result in a moment on the motor (see Figure 7). The moment will further result in a rotational deformation on motor shaft. Subsequently, the rotational deformation in motor will result in a linear displacement of the moving block along the ball screw's direction.

According to the Hook's law, the relation between rotational deformation of the *i*th motor, $\Delta\theta_m$, and applied moment on the *i*th motor, τ_m, can be written as,

$$\tau_{\mathrm{mi}} = K_{\mathrm{tor},i}\Delta\theta_{\mathrm{mi}} \quad (25)$$

where, the equivalent torsional stiffness of motor is denoted by K_{tor}. Also, the relationship between linear displacement of the moving blocks, Δq, and rotational deformation of motor is represented by,

$$\Delta q = \left(\frac{N l_b}{2\pi}\right)\Delta\theta_{\mathrm{m}} \quad (26)$$

where, l_b is the lead of the ball screw and *N* represents the gearbox transmission ratio. Using Equations (18), (25), and (26), equivalent linear spring which models the

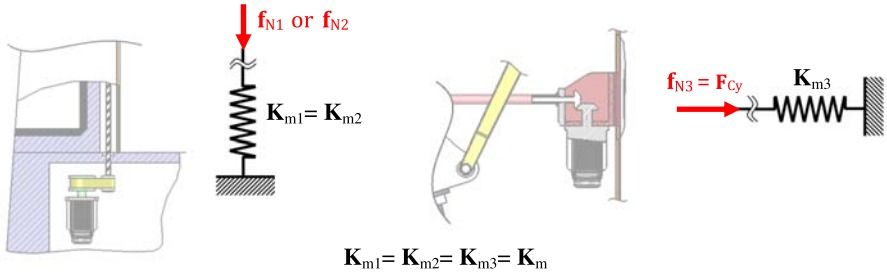

Figure 8. Lumped stiffness model of the motors.

stiffness of the ith motor can be determined. Since all three motors are assumed to be equal, we can write,

$$K_{\mathrm{mi}} = \frac{f_{Ni}}{\Delta q} = \left(\frac{2\pi}{Nl_b}\right)^2 K_{\mathrm{tor}} \tag{27}$$

Equivalent stiffness for this linear spring, K_{m}, determined from Equation (27), is modeled by COMBIN14 element type. Once the FEA model is developed, it can be used to obtain deflection of the end-effector anywhere within its workspace.

6. Numerical examples

6.1. Example 1: comparing the theoretical and FEA models

As stated earlier, in addition to other parameters, robot stiffness is a function of its configurations. Therefore, it is necessary to first solve inverse kinematics problem before performing stiffness analysis [1,5]. In this paper, a numerical example for verifying the theoretical stiffness model of the parallel manipulator is presented. First, a unique position and orientation for the end-effector is considered. Inverse kinematic of the robot is solved and essential kinematics values for stiffness are obtained. The structural and physical parameters of the robot are shown in Table 1. Assume that the following external wrench is applied to the end-effector at point P. For the external wrench expressed in {B} coordinate, we can write

$$\mathbf{W} = [500N\ 500N\ 0N.m]^T \tag{28}$$

The given inputs result in four solutions as given in Table 2 and graphically shown in Figure 3. The acceptable solution, solution #1, is depicted in Figure 9.

Results of the stiffness analysis are shown in Table 3 which includes results of the FEA model, and the analytical model as well as their difference.

As indicated in Table 3, the theoretical results closely follow the FEA results which verify the correctness of

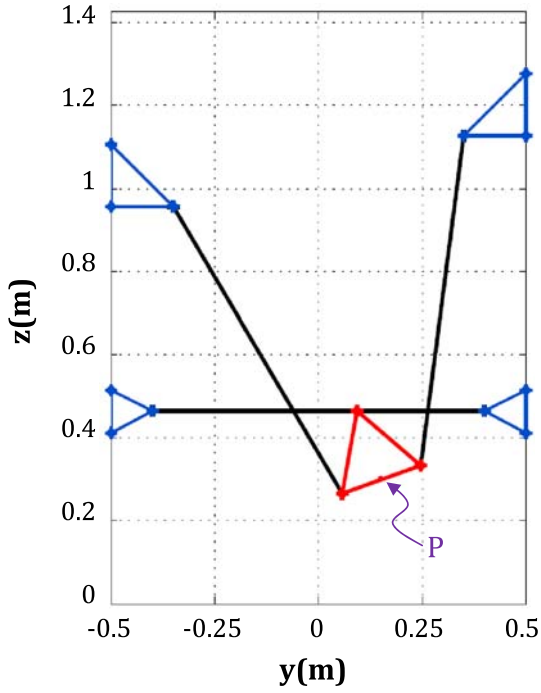

Figure 9. Result of inverse kinematic analysis-solution #1.

Table 1. Physical and structural parameters of the robot.

Parameters	Description	Values
a	OW (see Figure 3)	0.5 (m)
$h_1 = h_2$	AP (see Figure 3)	0.1 (m)
$b_1 = b_2$	Lengths of the two double bars	0.8 (m)
h_3	CP (see Figure 3)	0.1732 (m)
$d_1 = d_2$	N_1R_1 and N_2R_2 (see Figure 3)	0.15 (m)
d_3	(see Figure 3)	0.1 (m)
l_b	Lead of the ball screw	0.01 (m)
N	Gearbox transmission ratio	2
E	Elastic modulus of each double bar (ASTM-A242)	200 (Gpa)
k_{tor}	Equivalent torsional stiffness of ith motor [5,18]	3×10^4 Nm/rad

Table 2. Inputs/outputs values of inverse kinematic.

Inputs		Outputs (m)				
			Solution #1	Solution #2	Solution #3	Solution #4
y_{P}	0.15 (m)	q_1	1.1271	−0.4587	1.1271	−0.4587
z_{P}	0.30 (m)	q_2	0.9551	−0.4235	−0.4235	0.9551
φ	20 (deg)	q_3	0.3092	0.3092	0.3092	0.3092

Table 3. Results of stiffness analysis.

Inputs		Theoretical $\times 10^{-6}$	FEA $\times 10^{-6}$	$\|\|\delta\|\|$ diff. $\times 10^{-6}$
Translation (m)	δS_y	0.740	0.658	0.082
	δS_z	0.672	0.596	0.076
Orientation (deg)	$\delta S\varphi$	216.05	192.28	23.77

the theoretical stiffness model. The distributed model using energy method is clearly advantageous as it eliminates many of the simplifying assumptions and provides excellent agreement between the theoretical and the FEA models. The FEA simulation model, with both deformed and un-deformed shapes of the 3-axis robot, is shown in Figure 10.

6.2. *Example 2: stiffness in the z-direction*

The previous example considered a single configuration of the robot. In a CNC application, the robot is required to follow a trajectory and, therefore, deformation study throughout a trajectory is of importance. To study this, a circular and symmetrical trajectory, about z-axis, for the robot is considered and is divided into small segments. The orientation ψ is assumed to remain zero during the trajectory. The selected trajectory is shown in Figure 11.

At each point on this segment, a fixed external wrench, $\mathbf{W} = [500\,N\ 500\,N\ 0N.m]^T$, is applied to the end-effector at point P. Using Equation (13), deformations at that point are calculated. Results are shown in Figure 12 which shows both desired and deformed end-effector trajectories while spindle of the robot

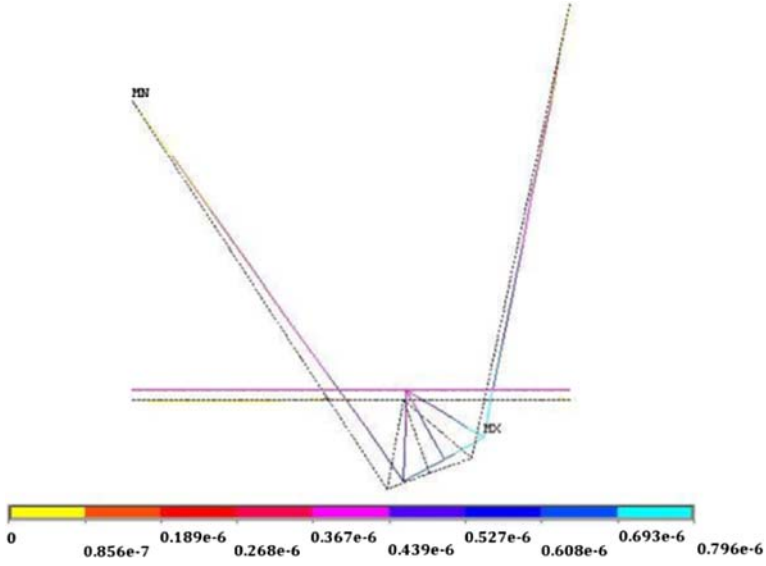

Figure 10. Deformed and un-deformed shape of the robot-FEA result.

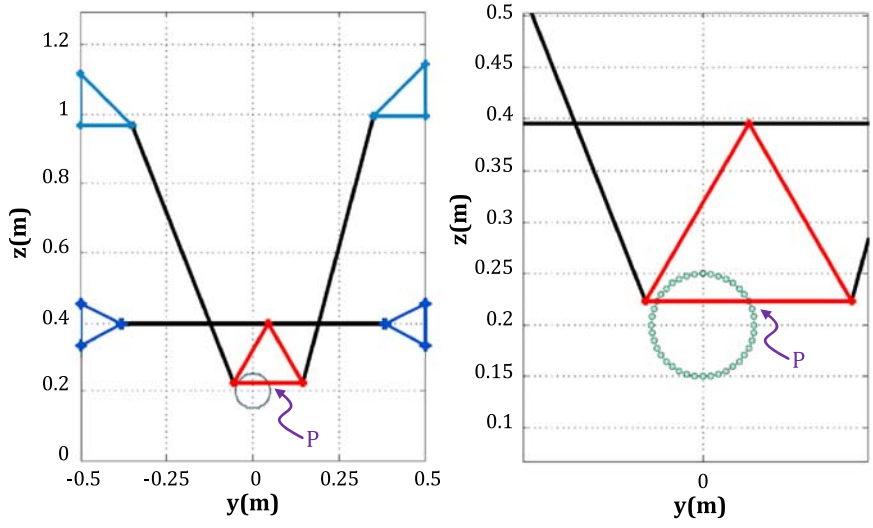

Figure 11. The circular and symmetrical trajectory.

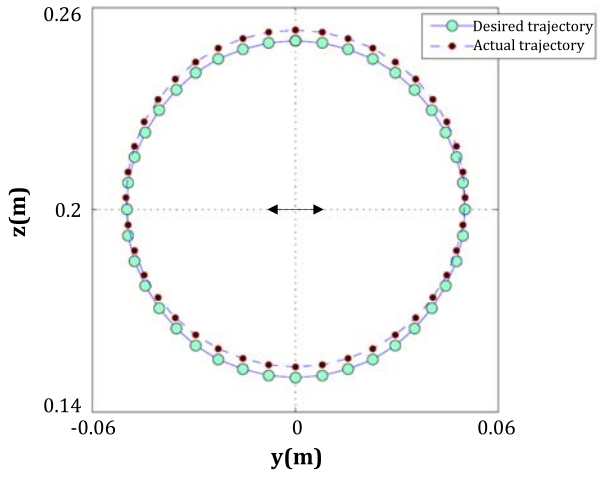

Figure 12. Desired and deformed trajectory of the end-effector, using constant values for $\varphi = 0$, Includes a multiplication factor of $10^{3.8}$.

follows the trajectory and experiences the fixed wrench. A trajectory with zero deflection is referred to as a desired trajectory where the robot is assumed to be fully rigid.

The better highlight the deflection through trajectory, difference between desired and deformed end-effector trajectories is calculated and shown in Figure 13. The maximum deflections for y, z, and ψ directions are 0.3×10^{-7} m, 5.157×10^{-7} m, and 7.332×10^{-6} deg, respectively. Note that the difference between the deformed and desired trajectories is very small. Therefore, to better graphically present this difference, Figure 12 uses a multiplication factor of $10^{3.8}$ for the difference between deformed and desired trajectories.

It should be noted that, as shown in Figure 13, the deflection is symmetrical. This result was intuitively expected as both the applied wrench and the selected trajectory result in a symmetrical deflection for the end-effector along its trajectory. The selected symmetrical trajectory plus the y direction external wrench can provide a sense of the robot stiffness in the y direction.

6.3. *Example 3: Stiffness in the y-direction*

To get a sense of stiffness in the y-direction, the same trajectory as in example 2 is selected. An external wrench is applied in the y-direction as $\mathbf{W} = [500\,N\ 0N\ 0.N.m]$. Deflection throughout this trajectory is calculated and shown in Figure 14. The maximum deflections for y, z, and φ directions are 6.9223×10^{-7} m, 0.3×10^{-7} m, and -1.9336×10^{-4} deg, respectively

By inspecting Figures 13 and 15, we can conclude that stiffness in both y and z directions are roughly equal. Such information can be used by a designer to better design the CNC machine.

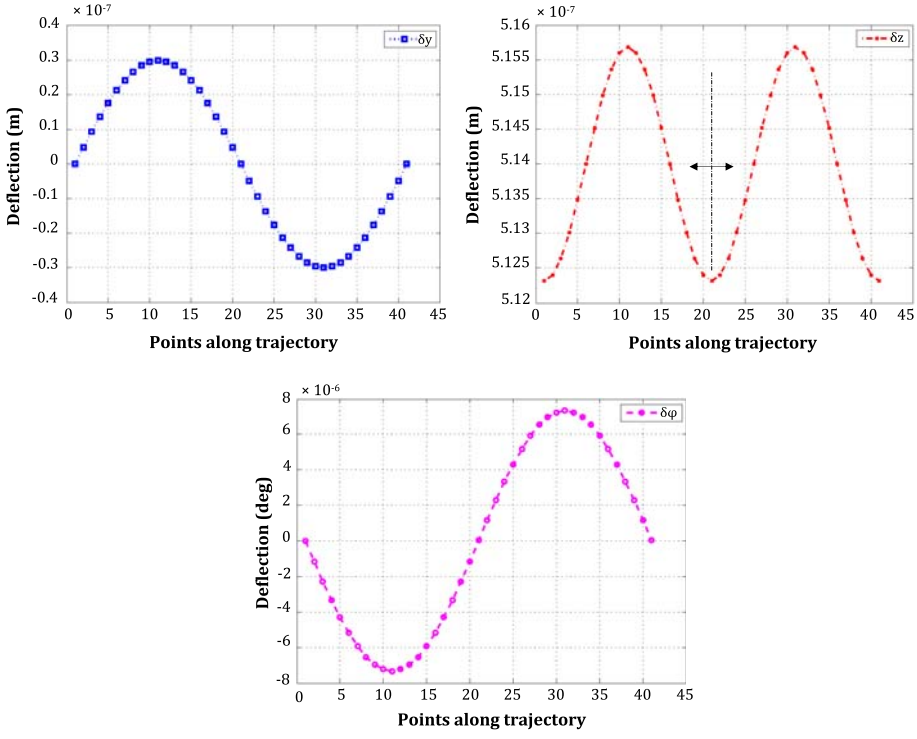

Figure 13. Deflection of point P along the circular trajectory with $F_y = M_x = 0$ and $F_z = 500$.

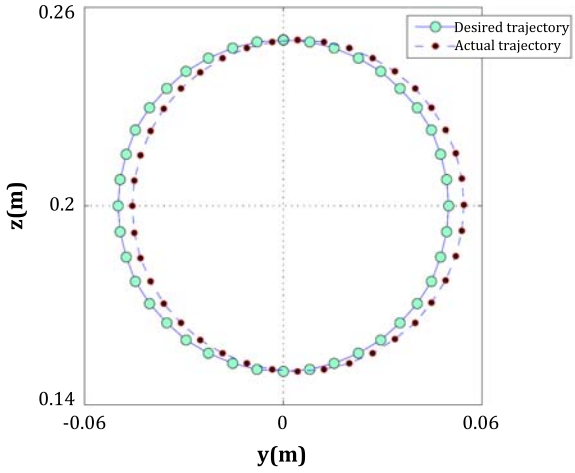

Figure 14. Desired and deformed trajectory of the end-effector, using constant values for $\varphi = 0$, Includes a multiplication factor of $10^{3.8}$.

6.4. Example 4: Stiffness in yz directions

Next, a similar circular trajectory, as before, but with its center shifted by 0.2 m in the y direction and a non-zero value for phi, $\varphi = \pi/20$, is selected. An external wrench of $\mathbf{W} = [500\,\text{N},\ 500\,\text{N}\ \ 0.\text{N.m}]^T$ is applied. Results are shown in Figure 16 which also shows both desired and deformed end-effector trajectories. The difference between desired and deformed end-effector trajectory for all points on the circular trajectory is shown in Figure 17.

As shown Figure 17, the maximum deflection for y and z directions are 7.90210^{-7}m and 7.598×10^{-7}m and φ direction is -2.13×10^{-4} deg, respectively. As before, we may also conclude that displacements in both y and z directions are roughly equal. It should also be noted that the deflection of the end-effector is asymmetrical. This was expected as the trajectory is nonsymmetrical with respect to the center of the workspace and includes a non-zero value for φ.

The calculated stiffness thus far refers to the 3-axis asymmetric robot and does not include the X–θ table. To calculate the overall stiffness of the hybrid CNC machine, the stiffness of the X–θ table should also be included.

7. Conclusion

In this paper, structural stiffness analysis of a new asymmetric planar parallel manipulator with a 2PRR−PPR kinematic chain is presented. First, structure of this robot as a tool holder for a 5axis hybrid CNC is introduced. Closed form inverse kinematics solution using closed-loop vector equations are derived. Upon solving these equations, essential kinematics values for stiffness analysis are obtained. Next, Stiffness analysis is presented. A method based on distributed model, calculation of strain energy of robot components, and Castigliano's theorem is used for the stiffness analysis. The method does not require any simplifying assumptions such as lumped model and ignoring bending effects in robot components. To verify results

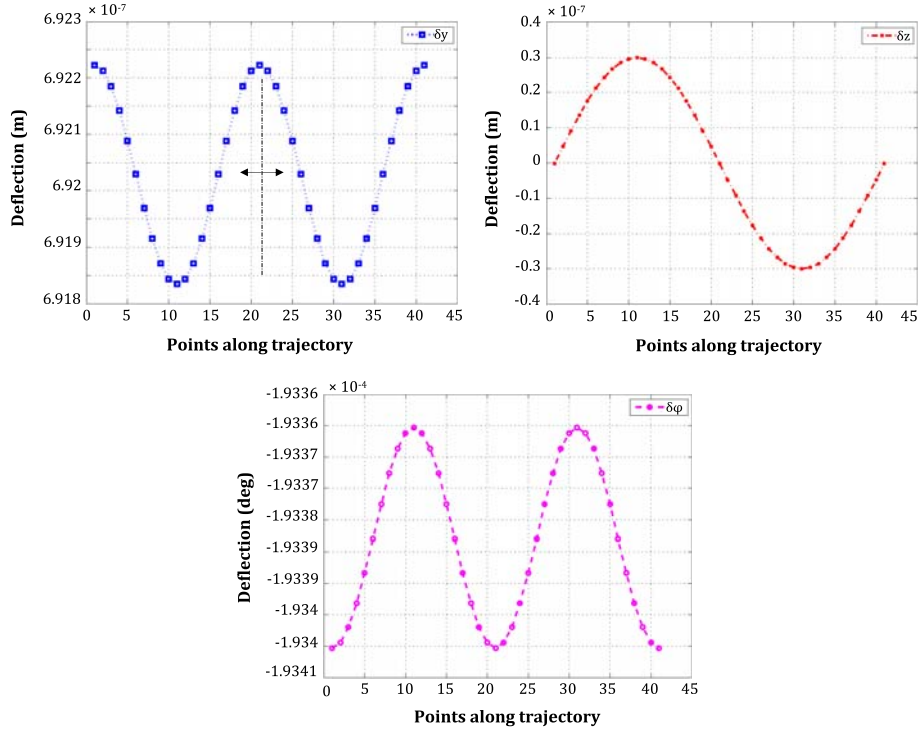

Figure 15. Deflection of point P along the circular trajectory with $F_z = M_x = 0$ and $F_y = 500$.

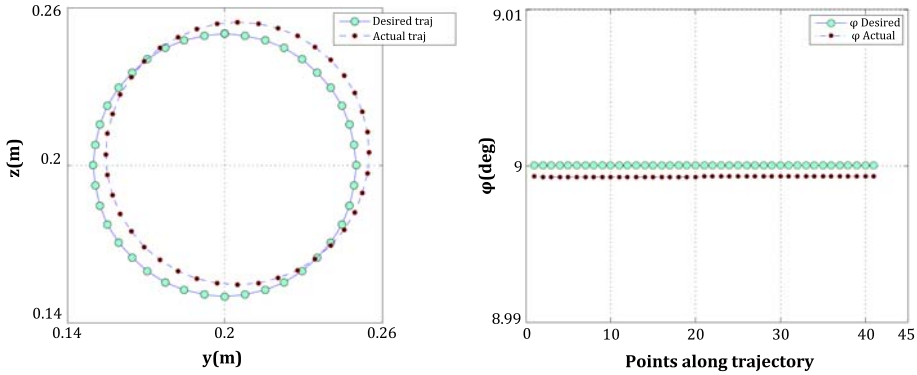

Figure 16. Desired and deformed trajectory of the end-effector, using constant values for $\varphi = \frac{\pi}{20}$, Includes a multiplication factor of $10^{3.8}$ for y–z graph and $10^{1.5}$ for φ diagram.

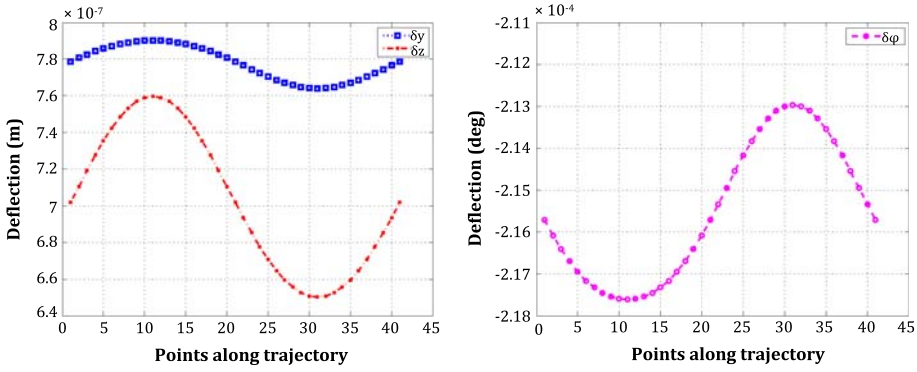

Figure 17. Deflection of point P along the circular trajectory with $F_y = 500$, $F_z = 500$ and $M_x = 0$.

of the analytical model, commercial FEA software is used to model the robot and several numerical examples are presented. It is shown that the robot stiffness varies with configuration and is roughly equal in the z and y directions. The close agreements between results indicate the correctness of the derived theoretical and FEM models.

This paper contributes by suggesting a new structure for a hybrid 5-axis CNC machine using a 3-axis asymmetric parallel manipulator and by obtaining a theoretical stiffness model using a method that eliminates many of the simplifying assumptions commonly used when calculating structural stiffness. The paper concludes with verification of the theoretical results.

Notes on contributors

Amir Rezaei received the M.Sc. degree from the Ferdowsi University of Mashhad (FUM), Mashhad, Iran, in 2011 and is currently a PhD candidate in Mechanical Engineering in the Robotics fields at FUM. Since 2010, he has been an active researcher in energy field and maintenance of the power plants, construction of the gas refinery in the South Pars Gas Field Development, Persian Gulf, Iran. Additionally, from 2007 to 2010, he has worked in the area of manufacturing and mechanical systems design. He is currently performing research in the area of parallel robots in the Center of Excellence on Soft Computing and Intelligent Information Processing (SCIIP), Ferdowsi University of Mashhad, Iran. His research interests include stiffness, kinematics and workspace, dynamics, singularity, visual tracking, manufacturing and control of parallel robots.

Alireza Akbarzadeh received his PhD in Mechanical Engineering in 1997 from the University of New Mexico in USA. He worked at Motorola, USA, for 15 years where he led R&D as well as automation teams. He joined the Ferdowsi University of Mashhad in 2005 and is currently an associate professor in the Mechanical Engineering Department. He has over 37 journal publications and over 55 conference papers. His areas of research include robotics (parallel robots, biologically inspired robots, bipedal robots, and rehabilitation robotics), dynamics, kinematics, control, automation, optimization as well as design and analysis of experiments. He is also a founding member of the Center of Excellence on Soft Computing and Intelligent Information Processing (SCIIP).

References

[1] Rezaei A, Akbarzadeh A, Enferadi J. Stiffness analysis of a spatial parallel mechanism with flexible moving platform. In: Proceedings of the ASME, 10th Biennial Conference on Eng. Sys. Design and Analysis, ESDA2010; Turkey: Mechanisms and Robotics; 2010. Vol. 3; p. 647–655.

[2] Patel AJ, Ehmann KF. Calibration of a hexapod machine tool using a redundant leg. Int. J. Mach. Tools Manufac. 2000;40:489–512.

[3] Son S, Kim T, Sarma SE, Slocum A. A hybrid 5-axis CNC milling machine. Precis. Eng. 2009;33:430–446.

[4] Rezaei A, Akbarzadeh A, Mahmoodi Nia P, Akbarzadeh T. MR. Position, Jacobian and workspace analysis of a 3-PSP spatial parallel manipulator. Robot. Comput. Integr. Manufact., RCIM [accepted for publication 2012 Nov 29].

[5] Enferadi J, Akbarzadeh A. Accuracy and stiffness analysis of a 3-RRP spherical parallel manipulator. Robotica. 2009;29:193–209.

[6] Kim JW, Kim KW, Kim HS, Kyung JH. Stiffness analysis and design of a 3-DOF parallel robot with one constraining leg. In: International Conference on Control, Automation and Systems (ICCAS 2007); 2007 Oct 17–20; COEX, Seoul, Korea. p. 2288–2293.

[7] Mahmoodi Nia P, Akbarzadeh A. Close form solutions for inverse and direct position analysis of a special 3-PSP parallel manipulator. In: 17th International Conference on Mechanical Engineering - ISME2009; 2009 May; University of Tehran, Iran.

[8] Gosselin CM. Stiffness mapping for parallel manipulators. IEEE Trans. Rob. Autom. 1990;6:377–382.

[9] Enferadi J, Akbarzadeh A. A novel spherical parallel manipulator: forward position problem, singularity analysis and isotropy design. Robotica. 2009;27:663–676.

[10] Majou F, Gosselin C, Wenger P, Chablat D. Parametric stiffness analysis of the orthoglide. Mech. Mach. Theory. 2007;42:296–311.

[11] Li Y, Xu Q. Stiffness analysis for a 3-PUU parallel kinematic machine. Mech. Mach. Theory. 2008;43:186–200.

[12] Xu Q, Li Y. An investigation on mobility and stiffness of a 3-DOF translational parallel manipulator via screw theory. Rob. Comput.-Integr. Manuf. 2008;24:402–414.

[13] Li S, Gosselin C. Stiffness analysis of 3-RRR planar parallel mechanisms based on CCT. In: 12th IFToMM World Congress; 2007; Besançon, France.

[14] Wang YY, Huang T, Chetwynd DG. Semi-analytical approach for stiffness estimation of pkm having complex machine frames. In: 12th IFToMM World Congress; 2007; Besançon, France.

[15] Wu J, Wang J, Wang L, Li T, You Z. Study on the stiffness of a 5-DOF hybrid machine tool with actuation redundancy. Mech. Mach. Theory. 2009;44:289–305.

[16] Chen JS, Hsu WY. Design and analysis of a tripod machine tool with an integrated Cartesian guiding and metrology mechanism. Precis. Eng. 2004;28:46–57.

[17] Koteswara Rao AB, Ravindra Varma U, Shankar Ganesh S. Workspace and stiffness analysis of a two degree of freedom translational parallel kinematic machine. In: Proceedings of the 2nd International Workshop on Fundamental Research for Parallel Mechanisms and Manipulators; 2008; Montpellier, France.

[18] Rezaei A, Akbarzadeh A, Akbarzadeh Totonchi MR. An investigation on stiffness analysis of a 3-PSP spatial parallel mechanism with flexible moving platform using invariant form. Mech. Mach. Theory. 2012;51:195–216.

[19] Arsenault M, Boudreau R. Synthesis of planar parallel mechanisms while considering workspace, dexterity, stiffness and singularity avoidance. ASME J. Mech. Des. 2006;128:69–78.

[20] El-Khasawneh BS, Ferreira PM. Computation of stiffness and stiffness bounds for parallel link manipulators. Int. J. Mach. Tools Manufac. 1999;39:321–342.